Journal of Sound and Vibration 330 (2011) 61–74

Contents lists available at ScienceDirect

Journal of Sound and Vibration

journal homepage: www.elsevier.com/locate/jsvi

Examination of mode shapes in an unstable model combustor

J.C. Sisco *, Y.C. Yu, V. Sankaran, W.E. Anderson

School of Aeronautics and Astronautics, Purdue University, 701 W Stadium Avenue, West Lafayette, IN 47907-2045, USA

ARTICLE INFO

Article history:
Received 22 April 2009
Received in revised form
11 July 2010
Accepted 16 July 2010
Handling Editor: P. Joseph
Available online 9 September 2010

ABSTRACT

The coupling between the fluid dynamics, heat addition, and the acoustics of a combustor system determine whether it is prone toward combustion instability. This paper presents results from a benchmark study of the eigenmodes in an unstable experimental combustor. The axisymmetric combustor configuration is representative of a number of practical systems and comprises an injector tube, geometric expansion into a combustion chamber, and a short converging nozzle. Instability limit cycle amplitudes ranged from 5% to nearly 50% of the mean 2.2 MPa pressure. Multiple harmonics were measured for the highly unstable cases. The model combustor was designed to provide a fairly comprehensive set of tested effects: sonic *vs* subsonic inlets; oxidizer tube lengths that were either quarter-wave, half-wave, or off-resonant acoustic equivalents to the combustion chamber; a significant injector mean flow with $Ma \sim 0.4$; and a varied combustion chamber length. The measured mode shape data were analyzed and reduced to provide comparison with results from a linearized one-dimensional Euler model, which included the effects of real boundary conditions, entropy generation, area change, and heat and mass addition, but did not include a model for unsteady heat addition. For low-amplitude instabilities, the measured resonance frequencies agreed with those calculated by the model for the injector tube-combustion chamber system. Resonance frequencies for the high-amplitude oscillation cases corresponded to the first longitudinal frequency of the combustion chamber and its integer multiples. Good quantitative agreement was obtained between computed and measured phase difference profiles, and mode envelopes agreed qualitatively. These results provide a basis for subsequent combustion response studies on the effects of unsteady heat addition.

© 2010 Elsevier Ltd. All rights reserved.

1. Introduction

Combustion instability is a phenomenon that is of enduring interest to the propulsion community [1]. Defined simply, unstable combustion occurs when resonant pressure oscillations in a combustion chamber are spatially and temporally in phase with oscillations in heat release and gas expansion due to unsteady combustion. A result is the amplification of the pressure oscillations—a phenomenon often explained by Rayleigh's criterion [2]. Rocket engine combustors are particularly susceptible to combustion instability because of their high energy release density close to an injector face, and because of low acoustic losses.

Despite a long history of liquid rocket combustion instabilities, an *a priori* predictive capability does not exist. This can be attributed to several factors, including: (1) the complexity of the problem, (2) the power required to capture the full

* Corresponding author.
E-mail address: jsisco@aurora.aero (J.C. Sisco).

0022-460X/$ - see front matter © 2010 Elsevier Ltd. All rights reserved.
doi:10.1016/j.jsv.2010.07.016

physics of the problem in computational simulations is not yet readily available, and (3) a lack of benchmark experimental data needed for model validation. This paper addresses the lack of benchmark experimental data by providing detailed measurements of axial mode shapes in an unstable model rocket combustor that was run at realistic operating conditions.

Compared to experimental studies of combustors used in airbreathing propulsion [3–11], model rocket combustor studies are few and lack detail [12–15]. Furthermore, whereas the airbreathing experiments used premixed gaseous propellants at low chamber pressure, rocket combustors use non-premixed propellants in nearly stoichiometric proportions at high pressures. The combination of denser energy release, more compact spatial modes, and higher sound speed result in stronger interactions between heat release and compression waves at considerably shorter time scales.

In this study, high-frequency pressure measurements were made at points throughout a combustor that exhibited moderate-to-strong instabilities at frequencies corresponding to the first through third longitudinal modes. The experimental combustor resembles practical ramjet, gas turbine, and rocket systems, including an injector tube through which propellants enter the chamber, a sudden expansion at the injector face, a cylindrical combustion chamber, and a sonic throat. Partial premixing of the propellants occurs in a short recess just upstream of the sudden expansion. The combustor has important specific similarities to combustion devices that are used in oxidizer-rich staged-combustion rocket engine cycles. In these combustors, the injector tube has the dual role of distributing propellants and acting as an acoustic resonator that damps chamber pressure oscillations [16].

Efforts were focused on: (1) determining the influence of the injector geometry on combustion system acoustics, (2) comparing measured dynamic pressure profiles and frequency content to calculated mode shapes and resonance frequencies, and (3) evaluating the influence of injector acoustics on selection of experimentally unstable frequencies. To provide a reasonably comprehensive set of benchmark measurements for model validation, frequency content and spatially resolved amplitudes of pressure oscillations are reported for six different test configurations that exhibited varying levels of instability. The test configurations encompass acoustically closed and open inlets (choked or subsonic, respectively), injector tube lengths ranging that ranged from quarter- to half-wave acoustic equivalents of the combustion chamber, and combustion chamber length.

Calculated mode shapes were obtained from a linearized, multi-domain, one-dimensional Euler analysis. The Euler model [17,18] incorporated effects due to mean flow, entropy waves, steady heat release, changes in cross-sectional area, mass addition, and physically realistic boundary conditions. Resonant frequencies and spatial mode shapes were predicted and compared to measurements in terms of spatial mode envelopes and phase angle. Comparison between the predicted and measured mode shapes indicate very good agreement in terms of nodal locations and phase angles, and lesser agreement with regard to the amplitude of the mode envelope. It is also shown that in several experimental configurations where the injector tube was designed to serve as a damping resonator for a particular mode were actually highly unstable at those same modes. This result illustrates the strong effect of unsteady heat addition, which was not modeled in the calculation.

Several important reasons exist to model the experiment with the linearized Euler equation (LEE) analysis. Firstly, instead of using admittance approximations commonly used in acoustic models, the LEE model naturally accounts for the inlet boundary effects of a subsonic flow. The effects of mean flow in the injector tube, where $Ma \sim 0.4$, and entropy production at interfaces are also included. Secondly, the comparison illustrates a validation process for which standards do not presently exist, and explores the selection and use of certain validating parameters. Thirdly, the validated model can be used to examine the dynamic system in detail; specifically, understanding the coupling between the oscillating pressure field in the combustor and the oscillating velocity field in the injector tube is key to understanding the mechanisms of combustion instability. Fourthly, the exact solution provided by the LEE analysis serves as verification for higher-order models, and a benchmark for simpler acoustic models. Finally, although the development of a combustion response model is outside the scope of this paper, the validated LEE model provides an efficient testbed for subsequent investigations of how the eigenmodes of the combustor system couple with fluid dynamics and unsteady heat addition.

2. Experimental details

The model combustor examined in this study (Fig. 1) was designed to encourage spontaneous longitudinal modes of instability by matching the acoustic modes of the injector tube to those of the combustion chamber. The configuration is similar to that of Miller et al. [19] who used a fully reflective upstream boundary with radial oxidizer inflow midway down the injector tube. In the present study, the oxidizer injector was modified significantly to specifically investigate the effects of tube geometry; to make it more straightforward to model; and to provide a closer resemblance to the open-inlet injector elements used in actual rocket engines [16].

A cross-section of the experimental combustor is shown in Fig. 1. The basic elements include an injector, or oxidizer, tube, a combustion chamber, and a sonic exit; each of these elements must be modeled to reasonably calculate system resonances. In actual practice the oxidizer tube is used as a damping device.

Fig. 2 shows how the oxidizer and fuel are injected into the combustor. Hot gaseous oxidizer is produced by flowing 90 wt% hydrogen peroxide, H_2O_2, through a catalyst bed. The product gas is at a temperature of approximately 1030 K, hot enough to auto-ignite the fuel, and is composed of about 42% oxygen gas, O_2, and 58% water vapor, H_2O, by weight. The oxidizer is delivered to a manifold, which measures 8.9 cm long by 5.1 cm in diameter, and then fed axially into the

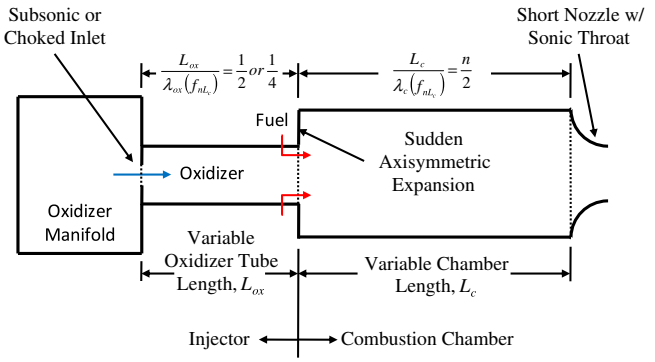

Fig. 1. Schematic of experimental combustor comprising oxidizer tube, axisymmetric fuel injection, combustion chamber, and short nozzle with sonic throat.

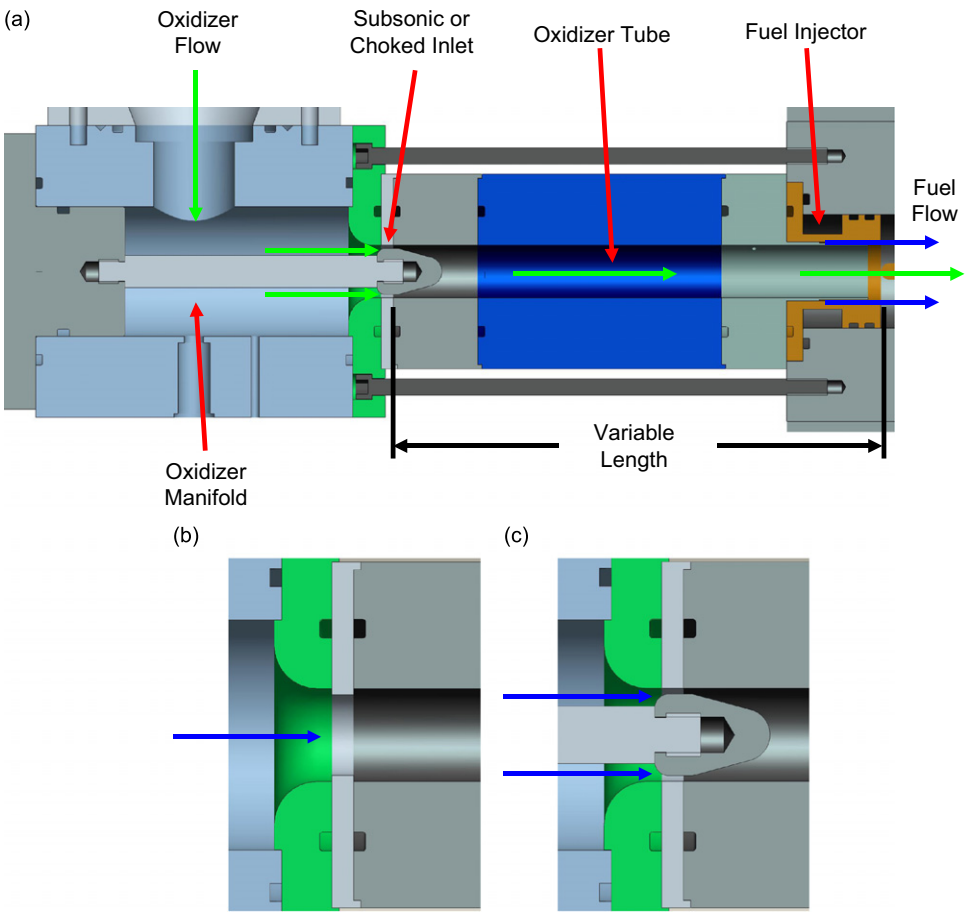

Fig. 2. Injector cross-section (a), and details of subsonic (b) and choked (c) inlets.

oxidizer tube. The oxidizer tube diameter was 2.05 cm and its length was adjusted discretely to provide either an acoustic 1/4-wave or 1/2-wave resonator. A swirling film of kerosene-based JP-8 fuel is introduced at the downstream end of the oxidizer tube by an injector containing a single row of four tangential orifices. A metal collar is used to initially protect the fuel. Propellants interact inside the tube over an exposed length of 0.51 cm. The partially mixed propellants enter the combustion chamber at an axisymmetric expansion. The combustion chamber length was set at either 38.1 or 63.5 cm, and its diameter was 4.45 cm. A short converging nozzle with a throat diameter of 2.08 cm was used to maximize reflection of pressure waves in the combustion chamber. The experiment was run at a nominal oxidizer-to-fuel mass ratio of 6.2 and a

nominal chamber pressure of 2.8 MPa. The nominal oxidizer manifold pressure was 8.3 MPa, and the nominal fuel injector pressure drop was about 1.1 MPa.

The combustor was oriented horizontally on the test stand, as shown schematically in Fig. 2, to facilitate chamber length adjustments. Oxidizer and fuel flow to the combustor were controlled by cavitating venturis designed with enough pressure margin to ensure cavitation, and constant flow rates, even under the most severe instabilities. Propellant tank ullage and venturi supply pressures were maintained at steady, fixed levels by high flow capacity, dome-loaded pressure regulators. Dry, gaseous nitrogen was used as a pressurant. A more complete description of the test facility may be found in Ref. [20].

The oxidizer tube lengths used in the experiment were set based on classical acoustic considerations neglecting the effect of mean flow in the tube. For the 38.1 cm chamber the oxidizer tube was chosen to act as either a half-wave or quarter-wave resonator for the chamber's first longitudinal (1L) mode, which was calculated to be about 1470 Hz. Consequently, the half-wave tube length was set at 23.4 cm while the quarter-wave tube was set to 11.7 cm. In the case of the 63.5 cm chamber the oxidizer tube lengths were set to act as half- and quarter-wave resonators for the chamber's second longitudinal (2L) mode of about 1765 Hz. This set the half-wave tube length at 19.1 cm and the quarter-wave tube length at 9.53 cm.

The injector is shown in detail in Fig. 2. Schematics of the subsonic and sonic inlets used in the present experiment are shown in Fig. 2b and c, respectively. The subsonic jet inlet was created by placing a sharp-edged orifice plate at the head end of the oxidizer tube, with a thickness of 4.75 mm and an orifice diameter of 17.8 mm to maintain a low inlet Mach number. The choked inlet was an inverted venturi. The plug had an entrance radius of 3.18 mm, a throat diameter of 18.0 mm, an expansion angle of 15°, and an overall length of 25.4 mm. In total, accounting for the two inlet designs, four oxidizer tube lengths, and two chamber lengths there were 16 different injector/combustor configurations available in this study; six are presented here.

The study injector elements have important resemblance to injectors used in oxidizer-rich staged-combustion rocket engines. Full-scale rocket test results have shown the primary importances of whether the inlet is subsonic or sonic, and whether the acoustic length of the oxidizer tube corresponds to a 1/4- or 1/2-wavelength of the combustor acoustics [16,21]. The subsonic inlet/half-wave oxidizer tube was shown to be the most stable element [16].

In each test a single high-frequency pressure transducer was located in the oxidizer manifold and at least two transducers were located in both the combustion chamber and oxidizer tube. Static measurements of mean pressure were also made in the oxidizer manifold, oxidizer tube, and combustion chamber. High-frequency pressure measurements were made with a mixture of PCB model 123A24 and 123M13 rocket motor piezoelectric transducers (AC-coupled) and Kulite model WCT-312 piezoresistive transducers (DC-coupled). All these transducers were manufactured with integrated electronics to provide output which is linear with pressure and were calibrated by the manufacturer to be accurate within ± 103 kPa ($\pm 0.5\%$ of full scale). Kulite transducer output was amplified using a Pacific Instruments model 9355 transducer amplifier module. Each transducer was water-cooled to protect sensitive electronics while the PCB models also contained a helium-bleed circuit to protect the sensing element. All high-frequency transducers were mounted in recessed ports with calculated resonance frequencies of greater than 10 kHz [22,23], and were sampled at 200 kHz. Static measurements were made with GE Druck model PMP1260 and PMP 4060 pressure transducers.

3. Thermoacoustic analysis and resonant frequency

A linearized Euler equation (LEE) model [17,18] was exercised to interpret test data in this study. The model provides an exact solution to the full one-dimensional Euler equations and is generalized for multiple domains. Boundaries that deviate from acoustically perfect conditions, such as mass inflow or entropy production, can also be incorporated into the model. Outputs include resonance frequencies, mode shapes, and growth (or decay) rates, α_i. Consequently, effects due to mean flow, entropy waves, steady and unsteady heat release, and area change, are included. The exact results from the LEE model can be used to evaluate the approximations implicit in acoustic analyses and to verify higher-order computations of idealized configurations.

In the LEE model flow is assumed to be compressible, unsteady, and inviscid and the fluid is assumed to be calorically perfect and ideal. Linear perturbations are assumed to propagate as one-dimensional plane waves and vortical disturbances are absent. Spatial variations in mean flow occur only in the streamwise direction and are assumed to be piecewise uniform. Changes in properties between domains are treated as discontinuities across which the conservation laws are applied. Mass, momentum, and energy source terms, which can be time dependent, are introduced at these interfaces. Further details of the formulation and verification of the Euler model for the longitudinal chamber considered here are given in Ref. [17].

In the present study, two different multi-domain analyses were used, depending on whether the inlets were subsonic or sonic. Regardless of the inlet type, the combustion chamber was broken up into two domains of equal cross-sectional area. Fluid in the first domain was assumed to be decomposed hydrogen peroxide to simulate the unreacted region downstream of the sudden expansion. This domain extended 3.8 cm from the injector face for all chamber lengths. Concentrated addition of the mean heat was stipulated at an infinitesimally thin interface between the two chamber domains. The second domain was assumed to contain combustion products, and extended to the start of the nozzle contraction;

consequently its length varied depending on chamber configuration. The concentrated combustion approximation has been assessed previously using three flame distribution profiles. The results indicate that concentrated combustion provides a close approximation to the current experimental configuration. The effects of flame distribution on resonant frequencies and spatial mode shapes are detailed in Ref. [18]. The location of the concentrated combustion has also been examined. The flame position in the LEE setup is calibrated using measured frequency from one experiment and is kept consistent between the investigated experimental configurations. At the exit of this domain the "short nozzle" approximation was used to simulate the effect of the choked nozzle on flow perturbations [22,24]. This approximation assumes isentropic flow and a constant Mach number at the throat.

Configurations with the choked inlet were modeled using a three-domain analysis: the first domain simulated the oxidizer injector tube and the second and third domains approximated the combustion chamber as described above. To simulate the choked inlet a mass inflow boundary condition, which sets volumetric flow rate and stagnation enthalpy constant, was applied at the entrance of the first domain. The length of the first domain varied with oxidizer tube length, and properties were those of decomposed hydrogen peroxide. In the limit of zero mean flow the inlet condition behaves as an acoustically closed boundary. It was assumed that the sonic/choked inlet effectively isolated the oxidizer manifold from oscillations occurring in the injector tube.

To analyze the subsonic inlet a nine-domain analysis was used to incorporate effects due to area change through the inlet. The first through fifth domains simulated the rounded contraction just upstream of the inlet, the sixth domain represented the inlet orifice, the seventh domain represented the oxidizer tube from the orifice to the injector face, and the eighth and ninth domains simulated the combustion chamber as described above. A domain-resolution study has been performed to ensure that five domains are sufficient to represent the rounded contraction upstream of the inlet. The axial length of the seventh domain was varied with variations in oxidizer tube length. To simulate the oxidizer manifold, stagnation pressure and temperature were fixed at the entrance of the first domain. Any two-dimensional flow effects occurring in the manifold were neglected in the analysis.

Resonance frequencies of the 38.1 cm combustion chamber configurations computed by the LEE model as a function of injector tube length are plotted in Fig. 3. For comparison the theoretical acoustic (closed inlet–closed exit) 1 and 2L modes, —, are also shown as solid lines. In Fig. 3 open circles identify the four choked inlet modes and open squares identify the four subsonic inlet modes as calculated with the LEE model. Due to the presence of the injector tube, more than two system resonance modes are calculated for each inlet configuration, e.g., for the subsonic inlet four different modes are present in this frequency and oxidizer tube length range. It is also interesting to note that for both inlets the computed frequencies are not necessarily integer multiples of one another as they are for theoretical chamber modes. For example, for an oxidizer tube length of 11.7 cm with a choked inlet the first computed resonance frequency is 1050 Hz while the next three computed modes are 1520, 2630, and 3620 Hz which are 1.4, 2.5, and 3.4 multiples of the 1050 Hz, respectively.

Also shown in Fig. 3 are the measured frequencies of the first and second modes from each test configuration with a chamber length of 38.1 cm. Varying levels of instability were measured. For highly unstable configurations, the measured frequencies of the higher modes are integer multiples of the first mode. In the lower amplitude cases the average frequencies of the second and third modes a bit lower, and closer to the system resonant frequency calculated by LEE. Fig. 3

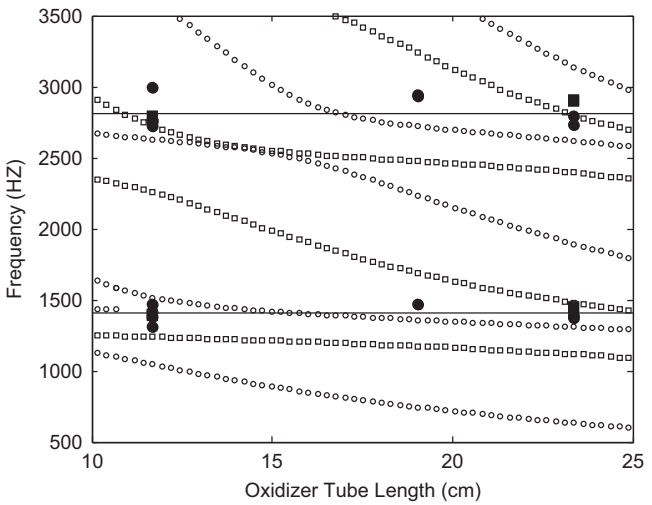

Fig. 3. System resonance frequencies calculated by a one-dimensional linearized Euler equation solver at a chamber length of 38.1 cm for choked, ○, and subsonic inlets, □, as a function of oxidizer tube length. Also shown are the first and second modes measured in each test run at a chamber length of 38.1 cm with the choked, ●, and subsonic jet, ■, inlets. Theoretical first and second chamber longitudinal modes are plotted as solid lines,—.

shows the measured frequencies of the first and second mode from each test configuration with a chamber length of 38.1 cm are similar to the theoretical acoustic (closed inlet–closed exit) 1 and 2L modes.

On average the theoretical combustion chamber mode frequencies were within 2.5% of measured frequencies, whereas the closest frequencies computed by the LEE model to those measured were within 5.9%. Frequencies computed by the LEE model more closely matched the second measured mode, within 4.6%, than the first measured mode, within 7.3%. Generally the LEE model matched measured frequencies better in tests with either the subsonic jet inlet or the 1/2-wave resonator tube length than those with either the choked inlet or the 1/4-wave tube. It should be noted that the deviation between actual gas properties and the ideal properties input to the model is a likely source of the discrepancy between measurement and calculation. Strong nonlinear behavior is another likely source. Still, good qualitative agreement is obtained and the differences themselves offer physical insight. The next section provides a more comprehensive discussion of the results in terms of mode shape and phase angle, and comparison with the analytical model.

4. Experimental results and comparison with model

The primary objective of this paper is to present detailed benchmark data on mode shapes in an unstable combustor that includes variations in inlet type (choked or subsonic), injector tube-combustion chamber resonance (quarter-wave, half-wave, and non-resonant), and chamber length. Both linear and highly nonlinear instabilities were measured. A summary of test data is shown in Tables 1 and 2, representative power spectral density plots are shown in Fig. 4, and mode shape and phase angle data are shown in Figs. 5–7. These all are discussed in this section.

Table 1
Nominal operating conditions of choked injector configurations.

Test designation	15-C920-01	15-C920-02	15-C460-01	15-C460-02	15-C460-03	15-C460-04	15-C750-01	15-C750-02	25-C750-03
Chamber length (cm)	38.1	38.1	38.1	38.1	38.1	38.1	38.1	38.1	63.1
Oxidizer tube length (cm)	23.4	23.4	11.7	11.7	11.7	11.7	19.1	19.1	19.1
L/λ (1L)—theo, no mf	0.51	0.51	0.26	0.26	0.26	0.26	0.42	0.42	0.25
L/λ (2L)—theo, no mf	1.03	1.03	0.51	0.51	0.51	0.51	0.84	0.84	0.50
Measured data									
P_c, x=11.4 cm (MPa)	2.59	2.61	2.63	2.64	2.65	2.66	2.70	2.69	2.67
C* efficiency (%)	90.0	90.4	91.6	91.4	91.9	91.8	94.8	92.8	94.4
Ox mdot (kg/s)	0.53	0.53	0.53	0.53	0.53	0.53	0.52	0.53	0.52
Fuel mdot (kg/s)	0.08	0.08	0.08	0.08	0.08	0.08	0.08	0.08	0.08
Mixture ratio	6.2	6.2	6.2	6.2	6.2	6.2	6.0	6.2	6.1
Ox man. (MPa)	7.94	8.04	8.12	8.14	8.16	8.20	7.97	8.04	8.03
Ox tube, $x=-4.95$ cm (MPa)	2.58	2.59	2.37	2.37	2.41	2.42	2.61	2.61	2.62
Fuel man. (MPa)	3.70	3.72	3.65	3.68	3.70	3.72	3.59	3.68	3.64
Primary frequency (Hz)	1390	1375	1415	1470	1385	1315	1470	1465	970
P'/P_c, x=1.27 cm (%)	39.4	25.2	4.9	8.2	7.4	4.9	34.2	54.9	24.7

Table 2
Nominal operating conditions of subsonic injector configurations.

Test designation	15-O920-01	15-O920-02	15-O460-02	15-O460-03
Chamber length (cm)	38.1	38.1	38.1	38.1
Oxidizer tube length (cm)	23.4	23.4	11.7	11.7
L/λ (1L)—theo, no mf	0.51	0.51	0.26	0.26
L/λ (2L)—theo, no mf	1.03	1.03	0.51	0.51
Measured data				
P_c, x=11.4 cm (MPa)	2.56	2.58	2.62	2.60
C* efficiency (%)	88.9	89.5	90.8	90.4
Ox mdot (kg/s)	0.53	0.53	0.53	0.53
Fuel mdot (kg/s)	0.08	0.08	0.08	0.08
Mixture ratio	6.2	6.2	6.2	6.2
Ox man. (MPa)	3.06	3.07	3.01	2.99
Ox tube, $x=-4.95$ cm (MPa)	2.55	2.55	2.67	2.59
Fuel man. (MPa)	3.68	3.70	3.80	3.70
Primary frequency (Hz)	1450	1440	1390	1395
P'/P_c, x=1.27 cm (%)	43.5	38.6	25.2	31.3

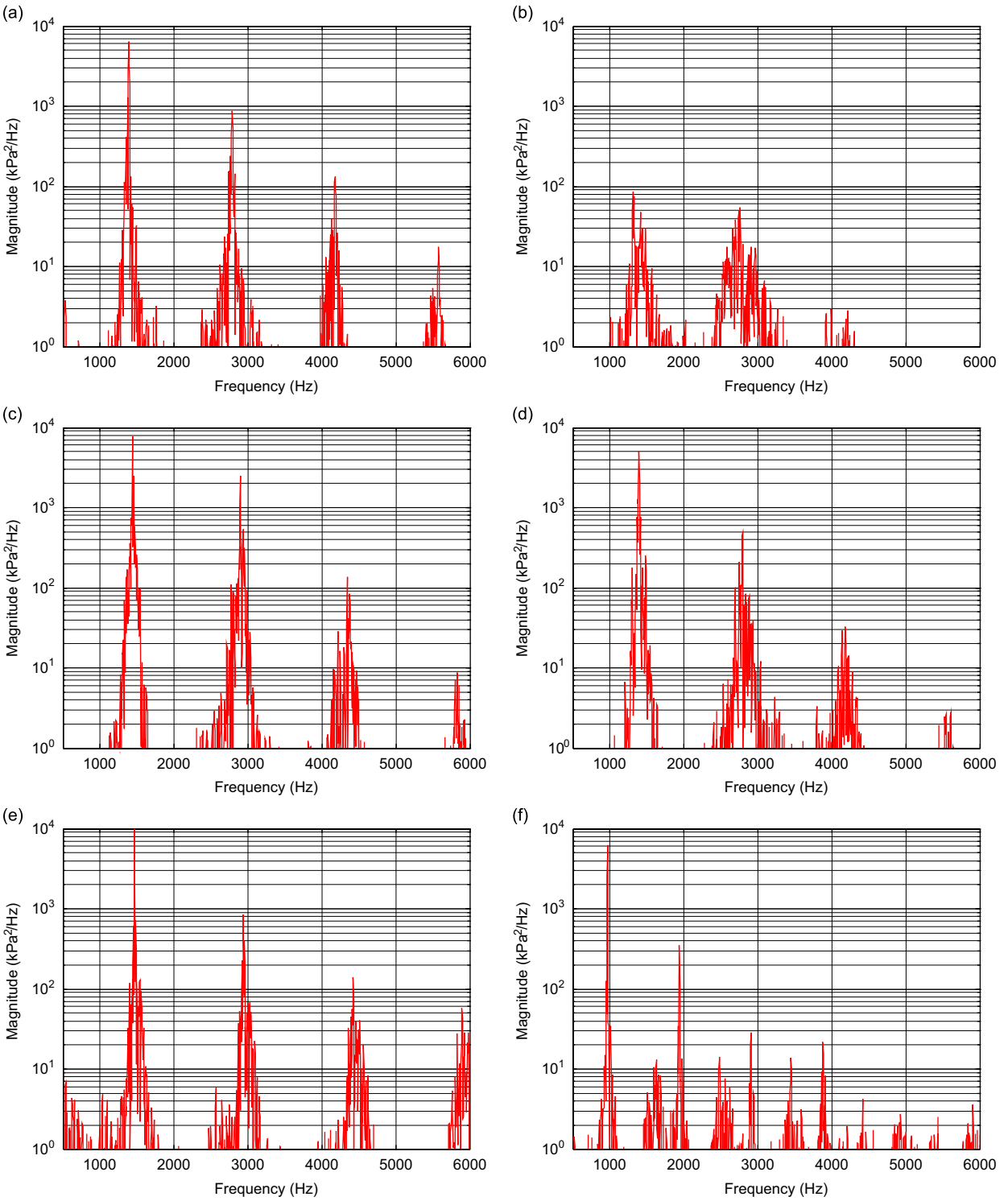

Fig. 4. Power spectral densities computed from 200 ms of dynamic pressure data measured 1.3 cm (0.5-in) downstream of the injector face in tests (a) 15-C920-01, (b) 15-C460-04, (c) 15-O920-02, (d) 15-O460-03, (e) 15-C750-01, (f) 25-C750-03. Each figure plots PSD magnitude in kPa^2/Hz on the y-axis versus frequency in Hz on the x-axis.

Test configurations are designated in the first row of each table. The first two numbers in the designation indicate the length of the combustion chamber in inches, the letter indicates the oxidizer inlet type (C=choked, O=subsonic jet), the three numbers attached to the inlet type indicate the oxidizer tube length in inches, and the last two numbers indicate the

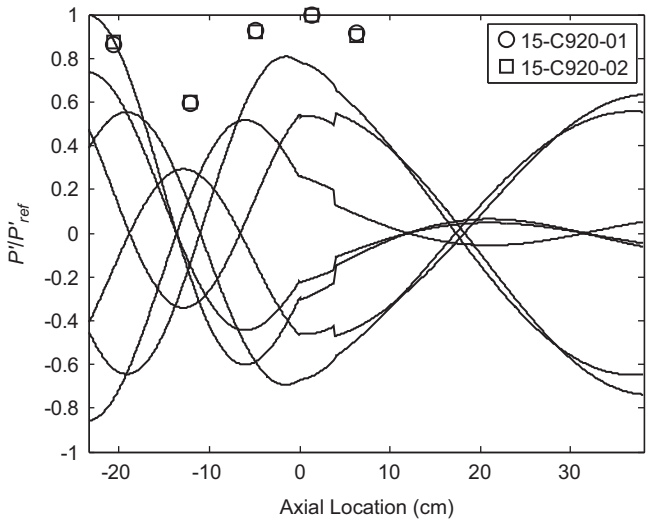

Fig. 5. Comparison of the measured axial dynamic pressure profile in tests 15-C920-01 (1390 Hz), ○, and 15-C920-02 (1375 Hz), □, to the corresponding pressure mode shape computed by the LEE model (1308 Hz), —, at seven instants during a single cycle. Discontinuities can be seen at the sudden expansion, $x=0$, and at the location of heat addition, $x=3.81$ cm.

test number. All the tests were run at nearly identical chamber pressure, P_c, and oxidizer-to-fuel mixture ratio. To assess repeatability most configurations were run two or more times. Instrumentation locations are referenced to the injector face, $x=0$. Locations in the oxidizer tube are designated by a negative x while those in the combustion chamber are denoted by a positive x.

Shown in the third and fourth row of each table are the theoretical oxidizer tube length to wavelength ratios based on the theoretical combustion chamber 1 and 2L mode frequencies. In most configurations this ratio is near one-half or one-quarter. The primary measured frequency and the estimated relative peak-to-peak pressure oscillation, P', are shown in the last two rows. The value of P' is calculated from a full-width, half-maximum (FWHM) analysis of the measurements at $x=1.27$ cm. This location was chosen for comparison because it typically showed the highest P' in the chamber. Spontaneous combustion instabilities with peak-to-peak variations ranging from 5% to 55% of mean chamber pressure were measured. In the FWHM analysis linear interpolation was used to estimate the frequencies at the half-power level of each peak in the power spectrum since the frequency resolution of the power spectrum was limited as described below.

Representative power spectral density plots from each configuration are shown in Fig. 4. Power spectral densities are computed based upon a 200 ms time slice of dynamic pressure data providing a frequency resolution of 5 Hz. The 38.1 cm combustion chamber with the quarter-wave injector tube with closed/choked inlet (Fig. 4b) was most stable, and the 38.1 cm chamber with the half-wave injector tube with open/subsonic inlet (Fig. 4c) was consistently most unstable. The other cases were unstable with peak-to-peak oscillations ranging from about 20% to 40% of mean chamber pressure. For all the above cases, the dominant modes corresponded to combustion chamber modes. The configuration with the off-resonant injector tubes (between quarter- or half-wave) shows a slightly more complicated power spectra (Fig. 4e). The 63.5 cm combustion chamber with the quarter-wave injector tube with choked inlet shows the most complex power spectra (Fig. 4f), with system (tube plus combustion chamber) modes apparent.

The measured unstable frequencies were within 7% of theoretical chamber longitudinal modes. Relatively stable operation, with $P'/P_c<10\%$, was observed with the quarter-wave oxidizer tube with choked inlet at a chamber length of 38.1 cm (Fig. 4b, test designation 15-C460). Stability parameters were quite repeatable in this configuration as the primary frequency varied by only 5% from the average of tests 15-C460-01 through -04 (1383 Hz) while P'/P_c was within 2% of the average (6.4%). Stability data were also repeatable in highly unstable tests, however in some cases, like 15-C750 (Fig. 4e), P'/P_c differed as much as 10% from the average. It should be note that the first tangential (1T) mode frequency for the combustor was computed at 15 kHz, while the first radial (1R) at about 30 kHz suggesting that the measured modes are in fact longitudinal.

A comparison between measured and calculated mode shapes for the 15-C920 configuration is shown in Fig. 5. This configuration was highly unstable at a frequency of about 1383 Hz with an estimated P'/P_c of approximately 32%. The amplitudes are computed for the primary modes, 1390 and 1375 Hz, from each test, respectively, through the FWHM integration approach. To facilitate comparison, both the measured oscillation amplitude and the computed mode shapes are normalized by their highest respective value.

Computed pressure mode shapes for the system resonances closest to the primary measured frequency in tests 15-C920-01 and -02 are denoted as solid lines, —, in Fig. 5. Each of the seven lines in the plot represents the spatial mode at a different instant in time during a single period of the 1308 Hz resonance. The modal lines are normalized relative to the highest calculated pressure oscillation amplitude, which in this case occurs at the oxidizer inlet or $x=-23.4$ cm.

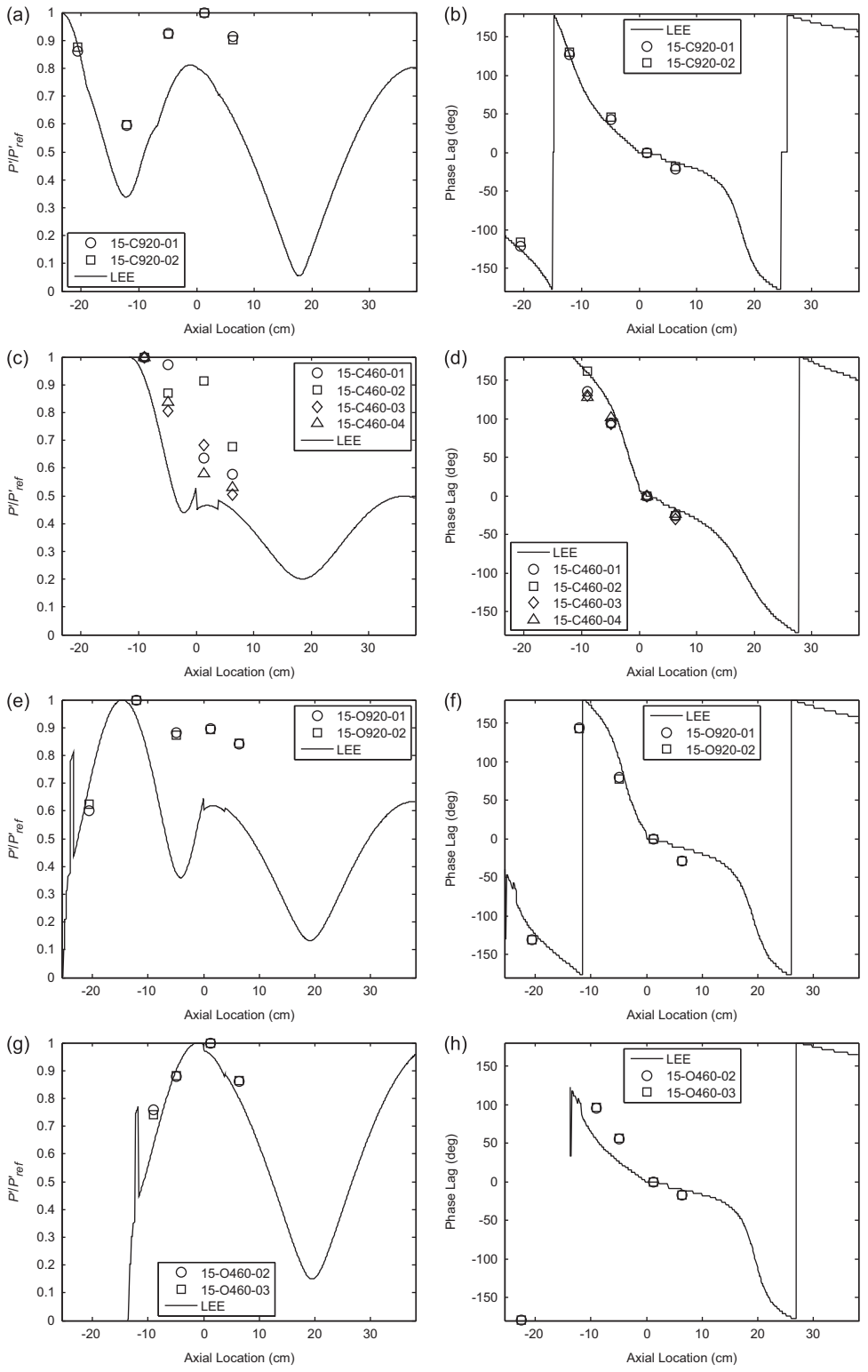

Fig. 6. Comparison between measurements and calculation of the axial dynamic pressure envelopes and phase lag profiles in test configurations 15-C920 (~1383 Hz), (a) and (b), respectively; 15-C460 (~1396 Hz), (c) and (d), respectively; 15-O920 (~1445 Hz), (e) and (f), respectively; and 15-O460 (xxx Hz), (g) and (h), respectively. Figures displaying mode shapes plot non-dimensional amplitude versus axial location in cm, while figures displaying phase information plot phase lag in degrees versus axial location in cm.

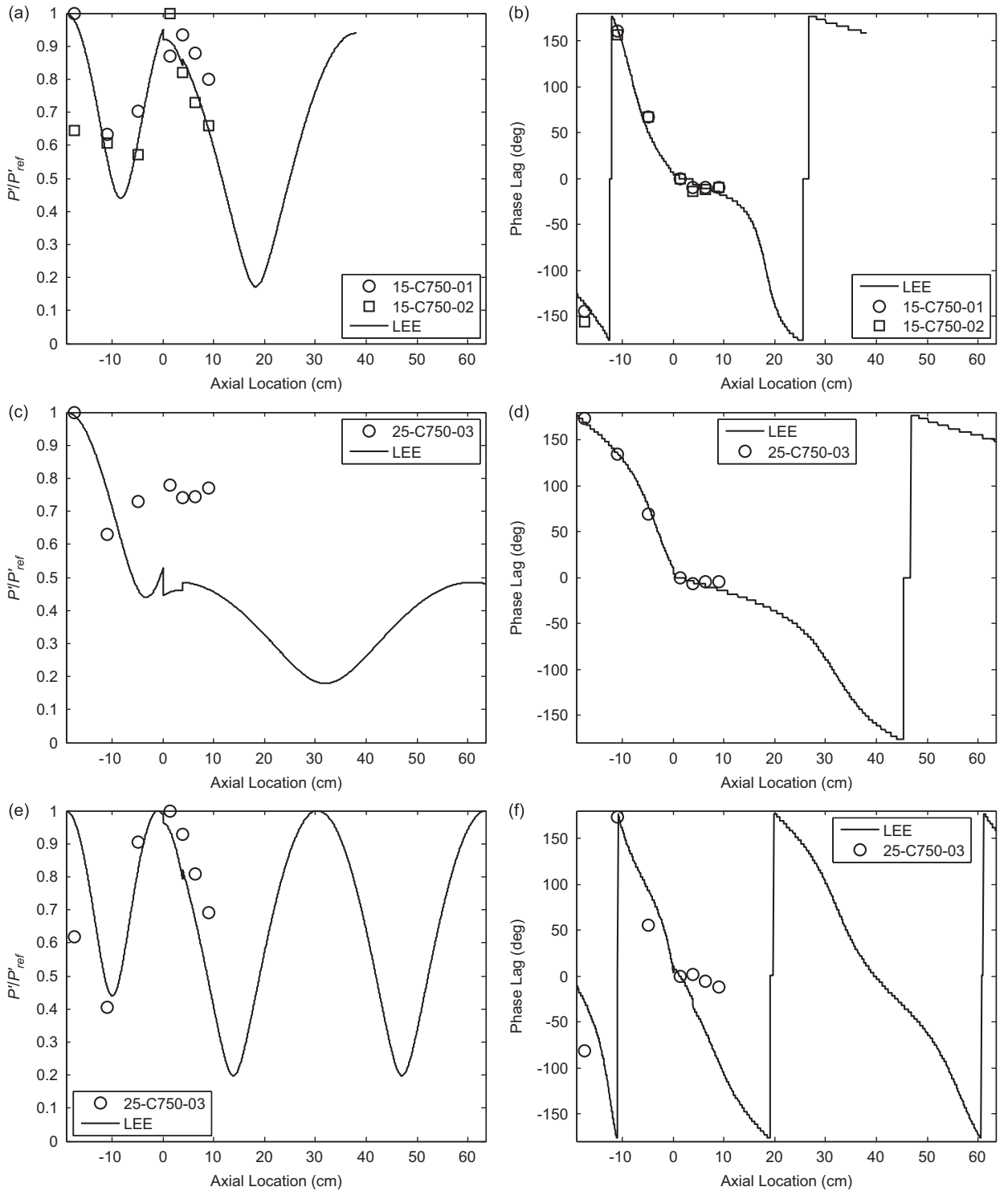

Fig. 7. Comparison between the measured axial dynamic pressure and phase lag profiles in test configurations 15-C750 (~1468 Hz), (a) and (b), respectively, 25-C750 (970 Hz), (c) and (d), respectively, and 25-C750 (1940 Hz), (e) and (f), respectively, to the envelope of the corresponding mode shape and phase profile computed by the LEE model. Figures displaying mode shapes plot non-dimensional amplitude versus axial location in cm, while figures displaying phase information plot phase lag in degrees versus axial location in cm.

Of particular note in Fig. 5 is the presence of discontinuities in the calculated modal lines at $x=0$ and 3.8 cm which are a consequence of the application of the conservation laws at the domain interfaces. Also of note is that the axial locations of the pressure anti-nodes and nodes oscillate in time over the course of the cycle, a consequence of mean flow effects on the propagation speed of disturbances in the combustor [17].

Since the measured dynamic pressure profiles displayed in Fig. 5 represent estimates of the peak-to-peak oscillation amplitudes it is more appropriate that they be compared to the envelope of the computed pressure mode shape. The computed envelope depicts the maximum amplitude of the pressure perturbation at each axial location computed over the course of a single cycle.

Comparisons can also be made through relative phase, or phase lag plots that show relative temporal locations of peak pressure between a reference location and any other location. For phase lag comparison, the reference position was selected to be 1.3 cm since a measurement was made at that axial location in every test. Relative phase measured pressure data were band-pass filtered around the frequencies of interest in each test using a fourth-order Butterworth filter. A search algorithm was used to identify temporal location of peaks in the pressure oscillation over a 200 ms time slice, which was the same slice used to compute P'. The relative difference between peaks was then computed throughout the time slice, and finally an average temporal deviation was estimated over that range. An identical algorithm was used to estimate the relative phase in LEE model output.

Fig. 6 shows measurements and calculations of mode shape and phase angle for the 38.1 cm combustion chamber comparing sonic/choked and subsonic/open-inlet cases for configurations using oxidizer tube lengths of 23.4 cm (half-wave resonator, $\lambda/2$) and 11.7 cm (quarter-wave resonator, $\lambda/4$). Results for the sonic/choked-inlet, half-wave resonator are shown in Fig. 6a and b; sonic/choked-inlet, quarter-wave resonator configuration in Fig. 6c and d; subsonic/open-inlet, half-wave resonator in Fig. 6e and f; and the subsonic/open-inlet, quarter-wave resonator in Fig. 6g and h. In Fig. 6 the positive x positions from 0 to 38.1 cm are in the chamber while the negative x positions are the oxidizer tube starting at the oxidizer inlet ($x=-23.4$ cm for the half-wave length tube and $x=-11.7$ cm for the quarter-wave length tube). The position $x=0$ is at the sudden axisymmetric expansion at the injector face.

A node is a point along a spatial wave where it has minimal amplitude and an anti-node is a point along a spatial mode where it has an amplitude maximum. All cases shown in Fig. 6 have a node near $x=20$ cm which is non-zero unlike classic acoustic modes. Calculations and measurement show that if the oxidizer tube is a half-wavelength tube (23.4 cm) the sonic/choked case has a non-zero node near $x=-12$ cm while the subsonic/open case has an anti-node at $x=-12$ cm. Calculations and measurement show that if the oxidizer tube is a quarter wavelength (11.7 cm) the sonic/choked case has a non-zero node near $x=0$ cm while the subsonic/open case has an anti-node at $x=0$ cm. Calculations and measurement show that the sonic/choked mass flow inlet produces an anti-node at the inlet boundary as shown in Fig. 6a and c. Calculations and measurement show that the subsonic/open-inlet produces a node at the inlet boundary as shown in Fig. 6e and g. Calculations show that the short nozzle exit conditions produce an anti-node at the exit boundary as shown in Fig. 6.

There is significant quantitative disagreement between the normalized dynamic pressure profile and the computed envelope at most locations. For example, at -12.1 cm, they differ by about 43%. Three primary reasons are offered for this disagreement: (1) inherently the linearized model is not able to accurately represent the behavior of this high-amplitude, nonlinear instability, which is also driving higher modes, (2) unsteady heat release has been neglected in the linearized model, and (3) the combination of the axial resolution in the dynamic pressure measurements and the normalization approach artificially amplifies the disparity.

A comparison between measured and calculated phase lags for the 15-C920 configuration is shown in Fig. 6b. The computed phase lags are for the primary modes, 1390 and 1375 Hz from each test of this configuration. A phase lag of zero degrees indicates that a peak in pressure oscillation at a particular axial location occurs at exactly the same time as that at the reference location (in phase), while a phase lag of $\pm 180^\circ$ indicates that peak pressure oscillations occur one-half-period before ($-$, lead) or after (+, lag) those at the reference location (out of phase).

Measured phase lags show that pressure oscillations near the oxidizer tube inlet lead those near the injector face by 120°. A 1/2-wave resonator should theoretically provide a 180° phase difference between the oxidizer inlet and injector face. Since pressure oscillations at the -12.1 cm location lag those at the reference location by about 128° it is assumed that this 180° phase difference occurs somewhere between the two locations in the upstream half of the oxidizer tube. We speculate that the shift downstream is due to any combination of area and property change effects near the injector face, mean flow effects in the oxidizer tube, and effects due the presence of a non-idealized oxidizer inlet boundary.

The quarter-wave configuration of Fig. 6c and d (15-C460) was marginally stable with an estimated P'/P_c of approximately 6.4% of mean chamber pressure; the most prominent measured mode was at frequency of about 1396 Hz. Again the mode shape and phase lag computed by LEE for the resonant mode closest to that measured (1515 Hz) is shown. The measured dynamic pressure profile suggests the presence of a 1/4-wave shape in the oxidizer tube in the 15-C460 configuration. Also of note is the large variation in measured amplitudes from test to test in configuration 15-C460, shown in Fig. 6c, which is unlike the data collected from configuration 15-C920, shown in Fig. 6a.

In Fig. 6d, both the data and the LEE model indicate a 180° phase difference between the inlet and the injector face in the 15-C460 (1/4-wave) configuration. This is contrary to idealized resonator theory, according to which this configuration should produce a 90° phase difference between the inlet and injector face. Also of note in Fig. 6d is that test-to-test

variation in the measured phase lag for configuration 15-C460 at each measurement location is significantly less than that of relative amplitude, Fig. 6c. Thus, relative phase may be a more consistent method of comparing measured data from test to test. Since it is less sensitive to the chosen reference location for normalization, the phase angle may be a more reliable comparator between test data and the LEE model.

Data from configuration 15-O920 (~1445 Hz) are shown in Fig. 6e and f. This half-wave subsonic configuration was highly unstable at a frequency of about 1445 Hz with an estimated P'/P_c of approximately 41%, ~10% higher than for 15-C920 (Fig. 6a). The subsonic inlet is an open boundary producing a pressure node at the oxidizer tube inlet, rather than a pressure anti-node as for the choked inlet. As such, the associated 1/2-wave mode shape in the oxidizer tube of the 15-O920 configuration should be exactly opposite to that of the 15-C920 (Fig. 6a).

The measured dynamic pressure profile shown in Fig. 6e for the 15-O920 configuration clearly reflects this anticipated result. For instance, at the −20.1 cm location near the subsonic inlet the relative amplitude is significantly lower, about 40%, than the corresponding measurement in the 15-C920 configuration. In addition, the mode shape traced out by this measurement along with those at the −12.1 and −5.0 cm locations indicates the presence of an anti-node near the mid-point of the oxidizer tube and a corresponding 1/2-wave mode shape which is exactly opposite in shape to that measured during tests run in the 15-C920 configuration.

The mode shape computed by the LEE model for configuration 15-O920, shown in Fig. 6e, qualitatively agrees with the measured dynamic pressure profile as both indicate reduced relative amplitude near the subsonic jet inlet and the presence of an anti-node near the mid-point of the oxidizer tube. The LEE model also indicates lower relative amplitude in the vicinity of the injector face in the 15-O920 configuration than the 15-C920, which is a consequence of the acoustic damping introduced by the 1/2-wave oxidizer tube with the subsonic inlet [16,21]. The model also confirms the presence of a chamber 1L mode in the combustion chamber. However, as in previous comparisons there is poor quantitative agreement between measured and computed relative amplitudes. In particular, the model predicts the presence of a pressure node at approximately −5.0 cm, but measured amplitudes do not indicate such a drastic decrease in amplitude at that location. The relative difference in amplitudes is on the order of 50%.

There is little difference between the measured phase lag profiles for configuration 15-O920 (Fig. 6f), and 15-C920 (Fig. 6b). The most significant measured deviation between the two configurations can be found at the −5.0 cm location where the phase lag is about 79° in the 15-O920 configuration and about 45° in the 15-C920 configuration. These observations are confirmed by the relative phase plots computed by the LEE model shown in Fig. 6f and b. There is good qualitative agreement between measured data and the LEE model, as the model predicts this phase difference at the −5.0 cm location. As in the 15-C920 configuration the measured and calculated phase difference between the oxidizer inlet and the injector face in the 15-O920 configuration is not 180°.

Data from configuration 15-O460 (~1393 Hz) are shown in Fig. 6g and h. This quarter-wave subsonic configuration was highly unstable at a frequency of about 1393 Hz with an estimated P'/P_c of approximately 28%. The measured mode shape for this configuration shown in Fig. 6g is in agreement with expectations. A pressure node is present at the injector inlet, and a quarter-wave shape is established in the injector tube. Also, there is a pressure anti-node present at the injector face (x=0 cm, Fig. 6g) with a relative amplitude higher by a factor of 1.11 than the measured value at the corresponding point for the 15-O920 configuration and higher by a factor of 1.66 than the measured value at the corresponding point for the 15-C460 configuration. LEE predictions are also in good quantitative agreement with measured mode shapes in this configuration.

Phase lags for the 15-O460 configuration are shown in Fig. 6h. In this case, the measured phase lag at the injector inlet is about 95°, which unlike the previously described configurations is very close to that predicted by resonator theory (90°). Quantitative agreement between measured phase lags and LEE predictions is somewhat poor in this case particularly near the injector inlet.

The effects of chamber length and non-resonant coupling between oxidizer tube and chamber on measured dynamic pressure and phase lag profiles are illustrated in Fig. 7 through a comparison of data corresponding to the primary modes from configurations 15-C750 (~1468 Hz) and 25-C750 (970 Hz). Corresponding mode shapes and phase lags computed by the LEE model for each of these configurations, 1359 and 925 Hz, respectively, are also shown in Fig. 7. In this case, both configurations were run with identical oxidizer tube lengths (19.1 cm) and sonic/choked inlets. 15-C750 was equipped with a 38.1 cm chamber length (end of Fig. 7a and b is x=38.1 cm) and 25-C750 with a 63.5 cm chamber length (end of plot 7c–f) is 63.5 cm). At these chamber lengths the oxidizer tubes behave differently; in the case of 15-C750 it is somewhere between a 1/2-wave and a 1/4-wave resonator for the chamber 1L mode, while for 25-C750 it should behave exactly as a 1/4-wave resonator for the chamber 1L mode. Both these configurations were highly unstable at frequencies close to their chamber 1L modes with estimated P'/P_c values of 34.2%, 54.9%, and 24.7%, respectively, from Table 1.

The measured dynamic pressure profile shown in Fig. 7a for the 15-C750 configuration indicates a 1/2-wave-like profile in the oxidizer tube. On the other hand, the measured oxidizer tube profile in 25-C750, Fig. 7c, reflects the anticipated 1/4-wave shape. There is a marked difference in the pressure profile at the head end of the combustion chamber (x=0 cm) between the two configurations. In the case of the 15-C750 configuration there is a 30% drop in the measured relative amplitude between the 1.3 cm and the 8.9 cm locations, while in the 25-C750 configuration the measured profile remains relatively flat within the first 8.9 cm of the injector face. This is most likely due to the increased wavelength of the 63.5 cm chamber 1L mode, which stretches out the anti-node at the injector face. The relative amplitudes at the head end of the combustion chamber are lower in magnitude on average for the 25-C750 configuration

than the 15-C750, which may be a result of the damping effect produced by the 1/4-wave oxidizer tube used for this long chamber length case.

The 1L mode shape computed by the LEE model shown in Fig. 7a and the 2L computed mode shape shown in Fig. 7c show good agreement with measured profiles at the head end of the chamber. Here, the increased wavelength computed by the LEE model in the 63.5 cm chamber for the 1L mode shown in Fig. 7c (25-C750 case) is clear when compared to that of the 38.1 cm chamber 1L mode shown in Fig. 7a (15-C750 case). The computed mode 1L mode shape for the 25-C750 configuration shown in Fig. 7c indicates a reduced relative amplitude at the head end of the combustion chamber (x=0 cm) (about 50%) as compared to the computed 1L mode shape for the 15-C750 configuration shown in Fig. 7a. The measured change at the head of the combustion chamber (x=0 cm) for the 25-C750 configuration (Fig. 7c) is not as substantial. The measured mode shape in the oxidizer tube of the 25-C750 configuration (Fig. 7c) is not well represented by the LEE model as the data suggest a node at about $x=-11$ cm before a flat region near x=0 cm rather than the LEE model calculated decrease leading to a calculated flat region near x=0 cm.

Despite the differences in mode shape between configurations 15-C750 and 25-C750 at the head end of the combustion chamber there is little difference between the measured phase lag profiles in that vicinity, as shown in Fig. 7b and d, respectively. In fact, the pressure oscillations within the first 8.9 cm of the chamber (x=0–8.9 cm) are almost completely in phase. However, there are some differences in phase between configurations in the oxidizer tube particularly at the -17.4 and -11.0 cm measurement locations due to the difference in mode shape there. Both the 15-C460 configuration (Fig. 6d) which has an oxidizer inlet at $x=-11.1$ cm and the 25-C750 configuration (Fig. 7d) which has an oxidizer inlet at $x=-19.1$ cm have an oxidizer tube which acts as a 1/4-wave resonator and show almost a 180° phase difference between the injector face (x=0 cm) and the oxidizer inlet. The phase lag profiles computed by LEE for both configurations show very good agreement with measured data even at the -11.0 cm location where there was some discrepancy in mode shape. Test-to-test variation in the dynamic pressure data between tests 15-C750-01 and -02 is significantly reduced in the phase lag plots.

Also shown in Fig. 7e and f are the measured dynamic pressure and phase lag profiles, respectively, for the first harmonic of the unstable mode (1940 Hz) in the 25-C750 configuration. These data are shown to illustrate that accurate mode shapes can be resolved at frequencies other than the primary unstable frequency. Since the oxidizer tube functions as a 1/4-wave resonator for the chamber 1L mode it should correspondingly function as a 1/2-wave resonator for the chamber 2L mode (or first harmonic of the 1L). Of course, a 2L mode shape, resembling a full wave, should be present in the combustion chamber.

The measured phase profile for the 1940 Hz mode of the 25-C750 configuration, shown in Fig. 7f, strongly resembles that of the primary mode in the 15-C750 configuration, Fig. 7b, at the head end of the combustion chamber and much of the oxidizer tube. The only major difference is in the phase lag at the -17.4 cm location which is about $-80°$ for the 25-C750 configuration compared to about $-150°$ for the 15-C750. As discussed previously, the theoretical phase difference between the oxidizer inlet and injector face for a 1/2-wave oxidizer tube is 180°, and this is another example where that was not the case. As shown in Fig. 7f, the phase lag profile computed by LEE is not in good agreement with that measured in the experiment particularly near the injector face. Finally, for unknown reasons, the phase lag profile is relatively flat within the first 8.9 cm of the injector face, while the model predicts a sharp drop off in phase.

5. Conclusions

This paper has summarized results from an examination of the stable and unstable modes produced by a single element model rocket combustor run at realistic operating conditions. Spontaneous longitudinal instabilities were driven by the unique characteristics of the injector tube/combustor configuration. Variations in oxidizer tube length (1/2- and 1/4-wave of chamber longitudinal mode) and oxidizer inlet geometry (choked and subsonic) were employed to evaluate the influence of injector geometry on observed stability. The combustor presented moderate-to-strong instabilities at frequencies corresponding to the first longitudinal mode in all but one experimental configuration.

Emphasis was placed on pressure mode shapes and phase differences measured in the injector tube and combustion chamber. Data analysis efforts were focused on: (1) determining the influence of the injector geometry on the acoustics in the combustion chamber, (2) comparing measured dynamic pressure profiles and frequency content to calculated mode shapes and resonance frequencies, and (3) evaluating the influence of injector acoustics on selection of experimentally unstable frequencies. Benchmark data were presented for validation purposes.

Results indicated that injector geometry, both tube length and inlet type, had a strong influence on pressure mode shapes and phase lag profiles in the oxidizer tube, but only minimal effect on the combustion chamber eigenmodes. The choked, 1/4-wave and subsonic, 1/2-wave oxidizer tube configurations, presumed to provide high acoustic damping, acted to reduce the relative amplitude of dynamic pressure oscillations at the head end of the combustion chamber. However, the mode shape and phase lag profiles in the chamber were unaltered and followed from traditional longitudinal modes. It was also found that oxidizer tube geometry did not have a significant influence on measured spectral content as all measured mode frequencies were within 2.5% on average (7% maximum) of those predicted by traditional longitudinal chamber acoustics. However, measured phase differences between the oxidizer inlet and injector face did not agree with traditional acoustics. For instance, 1/2-wave oxidizer tubes produced phase lags on the order of 80–125° rather than 180°,

and 1/4-wave tubes produced lags of about 180° rather than 90°, a consequence of the relatively high-speed flow ($Ma \sim 0.4$) in the injector tube. Results indicated that there was no clear link between observed stability and the presumed damping provided by the injector tube indicating that combustion dynamics, which are largely driven by the tube fluid dynamics, were the predominant factor in determining combustion instability.

A linearized Euler analysis was developed for the multiple domain combustor that incorporated effects due to mean flow and entropy waves, steady heat release, changes in cross-sectional area, and user defined boundary conditions on resonance frequencies and mode shapes. Computed resonance frequencies were generally within 6% of measured modes in all configurations. Mode shapes computed by the model showed good qualitative agreement with those measured in the combustor regardless of oxidizer inlet type, oxidizer tube length, or chamber length. Computed phase lags agreed quite well with measured values. Quantitative agreement between computed and measured mode shapes was poor in some cases. Two reasons were offered for the discrepancy: the general nonlinear behavior of the high-amplitude instabilities; and the artificial normalization procedure that was used to efficiently present and compare results. It was found that phase lag comparisons were a more robust approach to model validation due to their insensitivity to the spatial resolution of dynamic pressure measurements.

The detailed experimental data presented here serve as a validation set for stability modelers studying the unsteady dynamics of these complex configurations. Future work should emphasize measurement and analysis of the effects of unsteady heat addition.

Acknowledgments

This work was sponsored by the NASA Constellation University Institutes Project (CUIP) and NASA Graduate Student Researchers Program (GSRP). Further support for this work was obtained from the Air Force Office of Scientific Research (AFOSR): Modeling and Simulation of the Stability of ORSC Main Combustion Chambers, AFOSR Contract Number FA9550-08-C-0033, Dr. Mitat Birkan contract monitor. The authors would like to acknowledge the technical advice and other input from: Ms. Claudia Meyer and Dr. Jeff Rybak of Glenn Research Center; Dr. John Blevins of Marshall Space Flight Center; Dr. Douglas Talley of AFRL; Messrs. Enrique Portillo, Randy Smith, Nick Nugent, Rob McGuire, and Scott Meyer from Purdue University.

References

[1] F.E.C. Culick, V. Yang, Overview of combustion instabilities in liquid-propellant rocket engines, in: V. Yang, W.E. Anderson (Eds.), *Liquid Rocket Engine Combustion Instability, Vol. 169, Progress in Aeronautics and Astronautics*, AIAA, Washington, DC, 1995, pp. 3–37.
[2] Lord Rayleigh, *The Theory of Sound*, Dover Publications, New York, NY, 1945.
[3] V. Yang, Pressure Oscillations in Liquid-Fueled Ramjet Engines, PhD Thesis, California Institute of Technology, May 1984.
[4] V. Yang, F.E.C. Culick, Analysis of low frequency instabilities in a laboratory ramjet combustor, *Combustion Science and Technology* 45 (1986) 1–25.
[5] W.H. Clark, J.W. Humphrey, Identification of longitudinal acoustic modes associated with pressure oscillations in ramjets, *Journal of Propulsion and Power* 2 (3) (1986) 199–205.
[6] A.M. Laverdant, T. Poinsot, S.M. Candel, Mean temperature field effect on acoustic mode structure in dump combustors, *Journal of Propulsion and Power* 2 (4) (1986) 311–316.
[7] J.D. Sterling, E.E. Zukoski, Longitudinal mode combustion instabilities in a dump combustor, *25th AIAA Aerospace Sciences Meeting*, AIAA Paper 87-0220, Reno, Nevada, January 12-15, 1987.
[8] J.D. Sterling, Longitudinal Mode Combustion Instabilities in Air Breathing Engines, PhD Thesis, California Institute of Technology, May 1987.
[9] P.J. Langhorne, Reheat buzz: an acoustically coupled combustion instability – part 1: experiment, *Journal of Fluid Mechanics* 193 (1988) 417–443.
[10] G.J. Bloxsidge, A.P. Dowling, P.J. Langhorne, Reheat buzz: an acoustically coupled combustion instability – part 2: theory, *Journal of Fluid Mechanics* 193 (1988) 445–473.
[11] M.A. Macquisten, A.P. Dowling, Low-frequency combustion oscillations in a model afterburner, *Combustion and Flame* 94 (1993) 253–264.
[12] M.J. Zucrow, J.R. Osborn, An experimental study of high-frequency combustion pressure oscillations, *Jet Propulsion* 28 (10) (1958) 654–659.
[13] L. Crocco, J. Grey, D.T. Harrje, On the importance of the sensitive time lag in longitudinal high-frequency rocket combustion instability, *Jet Propulsion* 28 (12) (1958) 841–843.
[14] L. Crocco, J. Grey, D.T. Harrje, Theory of liquid propellant rocket combustion instability and its experimental verification, *ARS Journal* 30 (2) (1960) 159–168.
[15] B.A. Janardan, B.R. Daniel, W.A. Bell, B.T. Zinn, Measurements of reactive gaseous rocket injector admittances, *Combustion Science and Technology* 20 (1979) 185–193.
[16] M.L. Dranovsky, in: V. Yang, F.E.C Culick, D.G. Talley (Eds.), *Combustion Instabilities in Liquid Rocket Engines: Testing and Development Practices in Russia, Vol. 221, Progress in Aeronautics and Astronautics*, AIAA, Washington, DC, 2007, pp. 553–600.
[17] Y.C. Yu, J.C. Sisco, V. Sankaran, W.E. Anderson, Effects of mean flow, entropy waves, and boundary conditions on longitudinal combustion stability, *Combustion Science and Technology* 182 (2010) 739–776.
[18] Y.C. Yu, J.C. Sisco, C.L. Merkle, W.E. Anderson, V. Sankaran, The examination of spatial mode shapes and resonant frequencies using linearized Euler solutions, *37th Fluid Dynamics Conference and Exhibit*, AIAA Paper 2007-3999, Miami, FL, June 25–28, 2007.
[19] K. Miller, J. Sisco, N. Nugent, W. Anderson, Combustion instability with a single-element swirl injector, *Journal of Propulsion and Power* 23 (5) (2007) 1102–1112.
[20] J.C. Sisco, Measurement and Analysis of an Unstable Model Rocket Combustor, PhD Thesis, Purdue University, August 2007.
[21] C.H. Sohn, I. Park, S. Kim, H.J. Kim, Acoustic tuning of gas–liquid scheme injectors for acoustic damping in a combustion chamber of a liquid rocket engine, *Journal of Sound and Vibration* 304 (2007) 793–810.
[22] D.T. Harrje, F.H. Reardon (Eds.), *Liquid Propellant Rocket Combustion Instability*, NASA SP-194, Washington, DC, 1972.
[23] L.E. Kinsler, A.R. Frey, A.B. Coppens, J.V. Sanders, *Fundamentals of Acoustics*, fourth ed., John Wiley & Sons, New York, NY, 2000.
[24] B.T. Zinn, Longitudinal mode acoustic losses in short nozzles, *Journal of Sound and Vibration* 22 (1) (1972) 93–105.